Supplement of Earth Syst. Sci. Data, 17, 837–853, 2025
https://doi.org/10.5194/essd-17-837-2025-supplement

Supplement of

A new high-resolution multi-drought-index dataset for mainland China

Qi Zhang et al.

Correspondence to: Chiyuan Miao (miaocy@bnu.edu.cn)

Contents of this file

S1–S11. Methods

Figures S1–S8

S1. Methods: Correlation decay distance (CDD)

The ADW interpolation method used for this study was the modified Shepard's algorithm, which introduces the concept of correlation decay distance (CDD), also called correlation length scale or decorrelation length (Shepard, 1984; Dunn et al., 2020). The CDD is defined as the distance at which the correlation between one station and all other stations decays below 1/e, approximately corresponding to the significance level of 0.05 for the correlation within large samples (Jones et al., 1997; Harris et al., 2020). The number of stations for interpolating the target grid cell is well constrained by the CDD, thus improving the interpolation precision (New et al., 2000; Mitchell and Jones, 2005; Hofstra and New, 2009). For every station, correlations (r) and distances (x) for each variable are shown in Figure S1, and the ordinary least-squares method was used to fit an exponential decay function: $r = e^{-x/CDD}$, take the meteorological variable Wind (Figure S1a), for example, the estimated CDD is 361 km (95 % confidence interval: 361 km) at the 0.05 significance level.

S2. Methods: Standardized precipitation index (SPI)

The distribution of precipitation is generally not a normal distribution but a skewed distribution. Therefore, in precipitation analysis, drought monitoring, and assessment, the distribution probability Γ is used to describe the change of precipitation. The standardized precipitation index (SPI; McKee et al. 1993) is used to calculate the distribution probability Γ of precipitation within a certain period of time, perform normal standardization, and finally classify the drought level with the standardized precipitation cumulative frequency distribution.

$$f(x) = \frac{1}{\beta^{\gamma}\Gamma(\gamma)} x^{\gamma-1} e^{-x/\beta} \qquad x > 0 \tag{S1}$$

where $\beta > 0$ and $\gamma > 0$ are scale and shape parameters, respectively. β and γ can be obtained by the maximum likelihood estimation method: $\hat{\gamma} = \left[\frac{1}{4A}\left(1 + \sqrt{1 + \frac{4A}{3}}\right)\right]$, $\hat{\beta} = \frac{\bar{x}}{\hat{\gamma}}$, $A = lg\bar{x} - \frac{1}{n}\sum_{i=1}^{n} lgx_i$, where x_i is a precipitation data sample and $\bar{x}$ is the climate average of precipitation. After the parameters in the probability density function are determined, for the precipitation x_0 in a certain year, the probability of an event in which random variable x is less than x_0 can be calculated as follows:

$$f(x < x_0) = \int_0^{x_0} f(x)dx \tag{S2}$$

The event probability when the precipitation is 0 is estimated using the following formula:

$$F(x = 0) = m/n \tag{S3}$$

where m is the number of samples with precipitation of 0, and n is the total number of samples. The Γ distribution probability is normalized by the normal distribution function; that is, the probability values obtained by Equations (2) and (3) are substituted into the normalized normal distribution function:

$$F(x < x_0) = \frac{1}{\sqrt{2\pi}} \int_0^{x_0} e^{\frac{-Z^2}{2}} \tag{S4}$$

$$Z = SPI = S\left(t - \frac{c_0 + c_1 t + c_2 t}{1 + d_1 t + d_2 t^2 + d_3 t^3}\right) \tag{S5}$$

where $t = \sqrt{ln\frac{1}{F^2}}$, F is the probability of finding (2) or (3); and when $F > 0.5$, $F = 1-F$, $S = 1$, when $F \leq 0.5$, $S = -1$. The values of the coefficients are as follows: $c_0 = 2.515517$, $c_1 = 0.802853$, $c_2 = 0.010328$, $d_1 = 1.432788$, $d_2 = 0.189269$, and $d_3 = 0.001308$.

S3. Methods: Standardized precipitation evapotranspiration index (SPEI)

Both SPI and SPEI use a probability density function to fit time series. SPI uses a parametric Gamma distribution to fit cumulative monthly precipitation time series. SPEI is calculated similarly to SPI (Vicente-Serrano et al., 2010), using the cumulative difference between monthly precipitation and potential evapotranspiration (PET) to replace the precipitation variable, then using a three-parameter log-logistic distribution to fit the data, and then using the inverse cumulative probability density function of the standard normal distribution to convert to the drought index value (Li et al., 2020). First, the PET is calculated. The second step is to calculate the difference between precipitation (P) and PET, $D = P - PET$. The third step is to transform data D as SPI:

$$F(x) = \left[1 + (\frac{\alpha}{x-\gamma})^{\beta}\right]^{-1} \tag{S6}$$

T is the probability of a definite D value:

$$\mathrm{T} = 1 - F(x) \tag{S7}$$

For $T \leq 0.5$,

$$W = \sqrt{-2\ln(T)} \tag{S8}$$

$$SPEI = W - \frac{(c_2W + c_1)W + c_0}{[(d_3W + d_2)W + d_1]W + 1} \tag{S9}$$

For $T > 0.5$,

$$W = \sqrt{-2\ln(1-T)} \tag{S10}$$

$$SPEI = -\left(W - \frac{(c_2W + c_1)W + c_0}{[(d_3W + d_2)W + d_1]W + 1}\right) \tag{S11}$$

Values of coefficients are follows: c_0 = 2.515517, c_1 = 0.802853, c_2 = 0.010328, d_1 = 1.432788, d_2 = 0.189269, and d_3 = 0.001308.

S4. Methods: Evaporative demand drought index (EDDI)

In recent years, the indices for monitoring drought have mainly focused on water imbalance, because the physical actual evapotranspiration (AET)-based drought signal indices are used more and more frequently. These include the SPEI, soil water deficit index, evapotranspiration deficit index, remote sensing global drought severity index, etc. Although SPEI monitors drought on the basis of the difference between precipitation (P) and PET, PET is calculated on the basis of some formula or model; for example, PET obtained by Thornthwaite's method is estimated on the basis of average temperature, while reference crop evapotranspiration (ET_0) is not directly measured or represented by a separate index. An index based only on physical ET_0 measurements will have several advantages: first, the physically based ET_0 index does not need to consider the availability of surface water, because it focuses on the atmospheric water demand rather than the difference between surface water supply and demand. Second, it avoids the difficulties inherent in remote sensing data: some remote sensing data are affected by various factors, such as satellite remote sensing data being limited by cloud cover or the time interval when the satellite passes over the ground. This may lead to data delays or missing data. The physically based ET_0 index avoids the difficulties of relying on these data, because it does not need to use remote sensing data to infer water demand. EDDI was developed by Hobbins et al. (2016) as an indicator of atmospheric drying potential, which can indicate plant stress on the ground.

The rationale for this indicator is based on two main physical feedbacks between AET and ET_0 : under conditions of water resource constraint (protracted drought), AET and ET_0 change in opposite directions (Bouchet 1963), and under conditions of energy constraint at the onset of a sudden drought, they are in parallel (Fig. S8). Specifically, the magnitude of AET depends on the availability of energy (usually solar radiation, etc.) or water. If water limits evaporation, then atmospheric evaporation demand either plays a role in determining actual evaporation or is a reflection of it. For example, under non–water-constrained conditions, ET_0 estimates the upper limit of (energy-constrained) AET, whereas under water-constrained conditions, land–atmosphere feedbacks from AET lead ET_0 towards opposite or complementary directions. If we use the examples of persistent and sudden droughts, persistent droughts indicate persistent deficits in soil moisture (SM) and fluxes associated with land–air interfaces, where water constraints affect AET. However, "rapid droughts" (i.e., rapidly developing droughts caused by strong, transient meteorological/radiometric changes, such as increasing temperature, wind speed, radiation or moisture decrease, without substantial change in precipitation) tend not to be affected by water constraints. Nevertheless, ET_0 exhibited positive signals in both sustained and rapid droughts, indicating its value in monitoring droughts and as an early indicator of the development of drought conditions (Hobbins et al., 2016).

S5. Methods: Palmer drought severity index (PDSI)

PDSI is a drought index with clear physical meaning established by Palmer (1965).

It comprehensively considers many factors such as precipitation, soil moisture, runoff, and potential evapotranspiration; it can reflect the impact of pre-season precipitation and water supply and demand on later-period related factors; and it can effectively judge long-term drought conditions (Dai et al., 2004).

The water balance equation for water supply and demand to reach climate adaptation is as follows:

$$P' = \alpha_i PET + \beta_i PR + \gamma_i PRO - \delta_i Pl \tag{S12}$$

P' represents the climate-suitable precipitation, and α_i, β_i, γ_i, and δ_i are the water balance coefficients of each month *i* (*i* = 1, 2, 3, ..., 12), which can be defined as follows:

$$\alpha_i = \frac{\overline{ET_i}}{\overline{PET_i}}, \beta_i = \frac{\overline{R_i}}{\overline{PR_i}}, \gamma_i = \frac{\overline{RO_i}}{\overline{PRO_i}}, \delta_i = \frac{\overline{L_i}}{\overline{PL_i}} \tag{S13}$$

ET, *RO*, *R*, and *L* are respectively the actual evapotranspiration, actual flow, actual soil water replenishment, and actual soil water loss in month *i*. *PET*, *PRO*, *PR*, and *PL* are respectively the potential evapotranspiration, potential runoff, potential soil water replenishment, and potential soil water loss. In this model, $PR = AWC - (Ss + Su)$, $PRO = AWC - PR = S_s + S_u$, $PL = PL_s + PL_u$, $PL_s = min(PE, S_s)$, $PL_u = (PE - PL_s)S_u/AWC$, S_s is the initial effective upper soil water content, and S_u is the initial effective lower soil water content. According to the AWC data recommended by Li et al. (2023), we adopted the Global Gridded Surfaces of Selected Soil Characteristics data (https://daac.ornl.gov/cgi-bin/dsviewer.pl?ds_id=1006).

Water deficit (*d*) is the difference between actual precipitation (*P*) and climate-appropriate precipitation (P'). In order to make PDSI a standardized index, after finding the water deficit, we multiply it by the climate weight coefficient *K* of a given month in a given place, and thus obtain the water anomaly index *Z*, also known as the Palmer *Z* index, which indicates the degree of deviation between the actual climate dry–wet condition and its average water condition in a given month and place: $Z = dK$; the value of K is determined by the month and geographical location:

$$K_i = \frac{a}{\sum_{j=1}^{12} \overline{D_J}\, K_j'} K_i' \tag{S14}$$

The empirical constant a = 17.67 obtained by Palmer from the data of nine stations in seven states was revised to 16.84 according to the climate characteristics of China (Zhong et al., 2019), where $\sum_{j=1}^{12} \overline{D_J}\, K_j'$ is the average annual absolute moisture anomaly over the years, with j representing January to December;

$$K_i' = 1.6 \log_{10}\left(\frac{\frac{\overline{PET_\iota} + \overline{R_\iota} + \overline{RO_\iota}}{\overline{P_\iota} + \overline{L_\iota}} + 2.8}{\overline{D_\iota}}\right) + 0.4 \tag{S15}$$

where $\overline{D_\iota}$ the multi-year average of the absolute value of the moisture anomaly d in month i. Finally, the PDSI value for each month is calculated as follows:

$$X_i = pX_{i-1} + qZ_i \tag{S16}$$

where p and q are the duration factors that affect PDSI sensitivity. Palmer obtained p as 0.897 and q as 1/3 based on two stations in central Iowa and western Kansas, but we revised them to p = 0.755 and q = 1/1.63 on the basis of data from weather stations in China. PDSI is a cumulative index—that is, an index where each successive value is based on the previous value. Specifically, any given PDSI value (X_i) is the weighted sum of the previous PDSI value (X_{i-1}) and the current humidity anomaly Z_i. For example, the current PDSI value (X_i) is equal to q times the current water vapor outlier Z_i plus p times the previous PDSI value (X_{i-1}).

S6. Methods: Self-calibrating palmer drought severity index (SC-PDSI)

Based on PDSI, Wells et al. (2004) proposed and evaluated an SC-PDSI. Wells et al. (2004) believed that changing the ratio ($\widetilde{K}$) could solve the spatial inconsistency of PDSI without changing the way PDSI deals with seasonal climate changes.

$$\widetilde{K} = \frac{a}{\sum_{j=1}^{12} \overline{d}_J K_j'} K_i' \tag{S17}$$

Since $\sum_{j=1}^{12} \overline{d}_J K_j'$ can be approximately regarded as the annual sum of the average absolute value of Z ($\tilde{Z} = \sum_{j=1}^{12} \overline{d}_J K_j'$), and the value of a, 17.67 as obtained by Palmer, is the average value of $\tilde{Z}$ (i.e., the annual average sum of vapor anomalies), and since PDSI is based on cumulative vapor anomalies, so $\widetilde{K} = \frac{expected\ average\ PDSI}{observed\ average\ PDSI}$. The non-extreme value range of PDSI is defined as −4 to 4, but in practice this range is different. Palmer (1965) argues that if the PDSI were truly a standardized measure of drought severity, then values outside of that range (−4 to 4) would occur with roughly the same frequency. If the frequency of extreme events is f_e, then the f_eth percentile should be −4.00 and the (100 − f_e)th percentile should be 4.00. So $\widetilde{K} = \frac{expected\ feth\ percentile\ of\ the\ PDSI}{observed\ fe\ percentile\ of\ the\ PDSI}$. Defining an extreme drought as a "one in 50 year event" does not determine the percentage of PDSI values below −4.00, as it may last two months or two years. In this implementation, Wells et al. (2004) used an f_e value of 2%, which resulted in the following climate characterization equation:

$$K = \begin{cases} K'(-4\ /\ 2nd\ percentile), if\ d < 0 \\ K'(4\ /\ 98th\ percentile), if\ d \geq 0 \end{cases} \tag{S18}$$

Palmer found the duration factor empirically, based on the linear relationship between the length of time and severity of the most extreme droughts he studied in Kansas and Iowa. To estimate the severity of droughts, he summarized the Z-scores for severe droughts and derived the following linear relationship:

$$PDSI = -4.0 \Rightarrow \sum_{i=1}^{t} Z_i = -1.236t - 10.764 \tag{S19}$$

$$PDSI = -3.0 \Rightarrow \sum_{i=1}^{t} Z_i = -0.927t - 8.073 \tag{S20}$$

$$PDSI = -2.0 \Rightarrow \sum_{i=1}^{t} Z_i = -0.618t - 5.382 \quad (S21)$$

$$PDSI = -1.0 \Rightarrow \sum_{i=1}^{t} Z_i = -0.309t - 2.691 \quad (S22)$$

$$\sum_{i=1}^{t} Z_i = (0.309t + 2.691)X_i \quad (S23)$$

The linear relationship from (19) to (23) can be simplified to (24) for a given PDSI value $X_t = -4, -3, -2$, and -1.

$$\sum_{i=1}^{t} Z_i = (mt + b)\frac{X_t}{\mathrm{C}} \quad (S24)$$

It is not difficult to find that when $C = -4$, $m = -1.236$, and $b = -10.764$, (24) is equal to (19); (24) can also be derived in a generalized form as follows:

$$X_t = (1 - \frac{m}{m+b})X_{i-1} + \frac{C}{m+b}Z_t \quad (S25)$$

Thus, the persistence factor $p = (1 - \frac{m}{m+b})$, and $q = \frac{C}{m+b}$.

In practical analysis, because different regions have different sensitivities to precipitation events and some regions have different sensitivities to precipitation and non-precipitation periods, two sets of duration factors are needed. SC-PDSI establishes a separate duration factor for dry and wet periods, so that the sensitivity of the index depends on local climate and has different sensitivities to wetness and moisture deficit. We summarize the calculation steps of SC-PDSI as follows, after Wells et al. (2004):

(1) First, calculate moisture departures according to (12) and (13), $d = P - P'$;

(2) Calculate K according to K' in (15), and then calculate the moisture anomaly index, $Z = dK$;

(3) Calculate the index duration factor using the least squares method under extremely wet and extremely dry conditions: $\sum_{i=1}^{t} Z_i = mt + b$; this will give two sets of

parameters *m* and *b*. Calculate *m* and *b* according to the results of (13);

(4) Substitute *m* and *b* into Equation (25) to calculate PDSI;

(5) Recalculate *K* according to (18) after finding the 98th and 2nd percentiles of PDSI;

(6) Substitute the results of (10) into $Z = dK$ to get the new Z;

(7) Return to step 3 again to get the new *m* and *b*, and finally get SC-PDSI.

S7. Methods: Vapor pressure deficit (VPD)

Saturated vapor pressure is a function of temperature and can be directly calculated from temperature, as shown in the Tetens empirical formula (Allen et al., 1998):

$$e^0(T) = 0.6108\exp\left(\frac{17.27T}{T + 237.3}\right) \qquad (S26)$$

where $e^0(T)$ is the saturated water vapor pressure at temperature (kPa) at the air temperature T (°C). Since the above equation is a nonlinear function, for the average saturated vapor pressure with such a long interval at the monthly scale, if the average temperature is used to replace the daily maximum and minimum temperatures, the estimated value of the average saturated vapor pressure will be low, and the corresponding vapor pressure difference will be small. Therefore, the mean value of the saturated vapor pressure corresponding to the daily average maximum and minimum temperatures within the time interval is used for calculation (Li et al., 2014):

$$e_s = \frac{e^0(T_{max}) + e^0(T_{min})}{2} \qquad (S27)$$

where e_s is the average saturated vapor pressure (kPa), and T_{max} and T_{min} are the daily average highest and lowest air temperature (°C), respectively. The actual vapor pressure e_a (kPa) is calculated according to the monthly average relative humidity (φ_{mean}): $e_a = e_s \frac{\varphi_{mean}}{100}$, and VPD = $e_s - e_a$.

S8. Methods: Slope of the saturated vapor pressure

$$\Delta = \frac{4098 \times [0.6108 \times \exp\left(\frac{17.27T}{t + 237.3}\right)]}{(T + 237.3)^2} \tag{S28}$$

where Δ is the slope of the saturated vapor pressure temperature relationship ($\mathrm{kPa} \cdot {}^{\circ}\mathrm{C}^{-1}$)

S9. Methods: Psychrometric constant

$$\gamma = \frac{c_p P}{\varepsilon \lambda} = 0.665 \times 10^{-3} P \tag{S29}$$

$$P = 101.3 \times \left(\frac{293 - 0.0065z}{293}\right)^{5.26} \tag{S30}$$

where γ is the psychrometric constant ($\mathrm{kPa} \cdot {}^{\circ}\mathrm{C}^{-1}$); λ is the latent heat of evaporation ($2.45\ \mathrm{MJ} \cdot kg^{-1}$); ε is the molecular weight ratio of water to air (0.622); c_p is the specific heat of air at constant pressure ($1.013 \times 10^{-3} \mathrm{MJ} \cdot kg^{-1} {}^{\circ}\mathrm{C}^{-1}$); P is atmospheric pressure (kPa); and z is local elevation (m).

S10. Methods: Vapor pressure of the air

$$e^o(T) = 0.618 \exp\left(\frac{17.27T}{T + 237.3}\right) \tag{S31}$$

$$e_a = \frac{RH_{mean}}{100} [e^o(T)] \tag{S32}$$

$$e_s = \frac{e^o(T_{max}) + e^o(T_{min})}{2} \tag{S33}$$

where RH_{mean} is the mean daily relative humidity; T_{max} is the maximum temperature (°C); T_{min} is the minimum temperature (°C); and $e^o(T)$ is the saturation vapor pressure function (kPa).

S11. Methods: Net radiation at the ground surface

The first step is to calculate the extraterrestrial radiation (R_a). The daily extraterrestrial radiation at different latitudes during the year can be estimated from the solar constant, the magnetic declination of the sun, and the day's position during the year.

$$R_a = \frac{24 \times 60}{\pi} G_{sc} d_r [\omega_s \sin(\varphi) \sin(\delta) + \cos(\varphi) \cos(\delta) \sin(\omega_s)] \tag{S34}$$

where R_a is extraterrestrial radiation (MJ $\cdot\, m^{-2} day^{-1}$); G_{sc} is the solar constant and takes the value of 0.082 (MJ $\cdot\, m^{-2} min^{-1}$); d_r is the average distance between the Earth and the sun, calculated by equation (35); δ is the magnetic declination of the sun (rad), calculated by equation (36); φ is latitude (rad); and ω_s is the sunset hour angle, calculated by equation (37).

$$d_r = 1 + 0.033 \cos\left(\frac{2\pi}{365} J\right) \tag{S35}$$

$$\delta = 0.408 \sin\left(\frac{2\pi}{365} J - 1.39\right) \tag{S36}$$

where J indicates the day order, ranging from 1 to 365 or 366.

$$\omega_s = \arccos[-\tan(\varphi) \tan(\delta)] \tag{S37}$$

If the observed value of solar radiation R_s is not available, it can be obtained from the formula for the relationship between solar radiation and extraterrestrial radiation and relative insolation:

$$R_s = \left(a_s + b_s \frac{n}{N}\right) R_a \tag{S38}$$

where *n* is actual sunshine hours (h); *N* is the maximum possible sunshine hours; and a_s and b_s vary with atmospheric conditions (humidity, dust) and the sun's magnetic declination (latitude and month). When there are no actual solar radiation data and empirical parameters to use, it is recommended to use a_s = 0.25 and b_s = 0.5.

Net short-wave radiation at the surface is calculated by the balance of received and reflected solar radiation:

$$R_{ns} = (1 - \alpha)R_s \tag{S39}$$

where R_{ns} is net solar radiation or shortwave radiation (MJ $\cdot\, m^{-2}day^{-1}$); and α is albedo, where the albedo of the reference crop of green grassland is 0.23.

When near sea level or when empirical parameters are available for a_s and b_s, the clear-sky solar radiation is calculated by the following formula:

$$R_{so} = (a_s + b_s)R_a \tag{S40}$$

where R_{so} is clear-sky solar radiation (MJ $\cdot\, m^{-2}day^{-1}$).

The net long-wave radiation (R_{nl}) is calculated as follows. Long-wave radiation is proportional to the 4th power of the absolute surface temperature, and this relationship can be quantified by the Stefan-Boltzmann law. However, due to atmospheric absorption and downward radiation, the net energy flux at the surface is less than the value calculated using the Stefan-Boltzmann law. Water vapor, clouds, carbon dioxide, and dust all absorb and emit long-wave radiation, and their concentrations should be known when estimating net expended radiation fluxes. Due to the large influence of humidity and cloud cover, these two factors are used to estimate the net expenditure flux of long-wave radiation using the Stefan-Boltzmann law, and the concentration of other absorbers is assumed to be constant:

$$R_{nl} = \sigma[\frac{{T_{max,K}}^4 + {T_{min,K}}^4}{2}](0.34 - 0.14\sqrt{e_a})(1.35\frac{R_s}{R_{so}} - 0.35) \tag{S41}$$

where σ is the Stefan-Boltzmann constant with a value of 4.903×10^{-9} (MJ $\cdot$ $K^{-4}m^{-2}day^{-1}$); $T_{max,K}$ is the highest absolute temperature in a day (24 hours) in Kelvin (K; K = °C + 273.16); $T_{max,K}$ is the lowest absolute temperature in a day (24 hours) in Kelvin; and $(0.34 - 0.14\sqrt{e_a})$ is the corrected term for air humidity: if the air humidity increases, the value of this term will become smaller; $(1.35\frac{R_s}{R_{so}} - 0.35)$ is the revised term for the cloud cover, and if the amount of cloud increases, R_s will decrease and the value of this term will decrease accordingly.

The net radiation R_n is the difference between the incoming short-wave net radiation R_{ns} and the outgoing long-wave net radiation R_{nl}:

$$R_n = R_{ns} - R_{nl} \tag{S42}$$

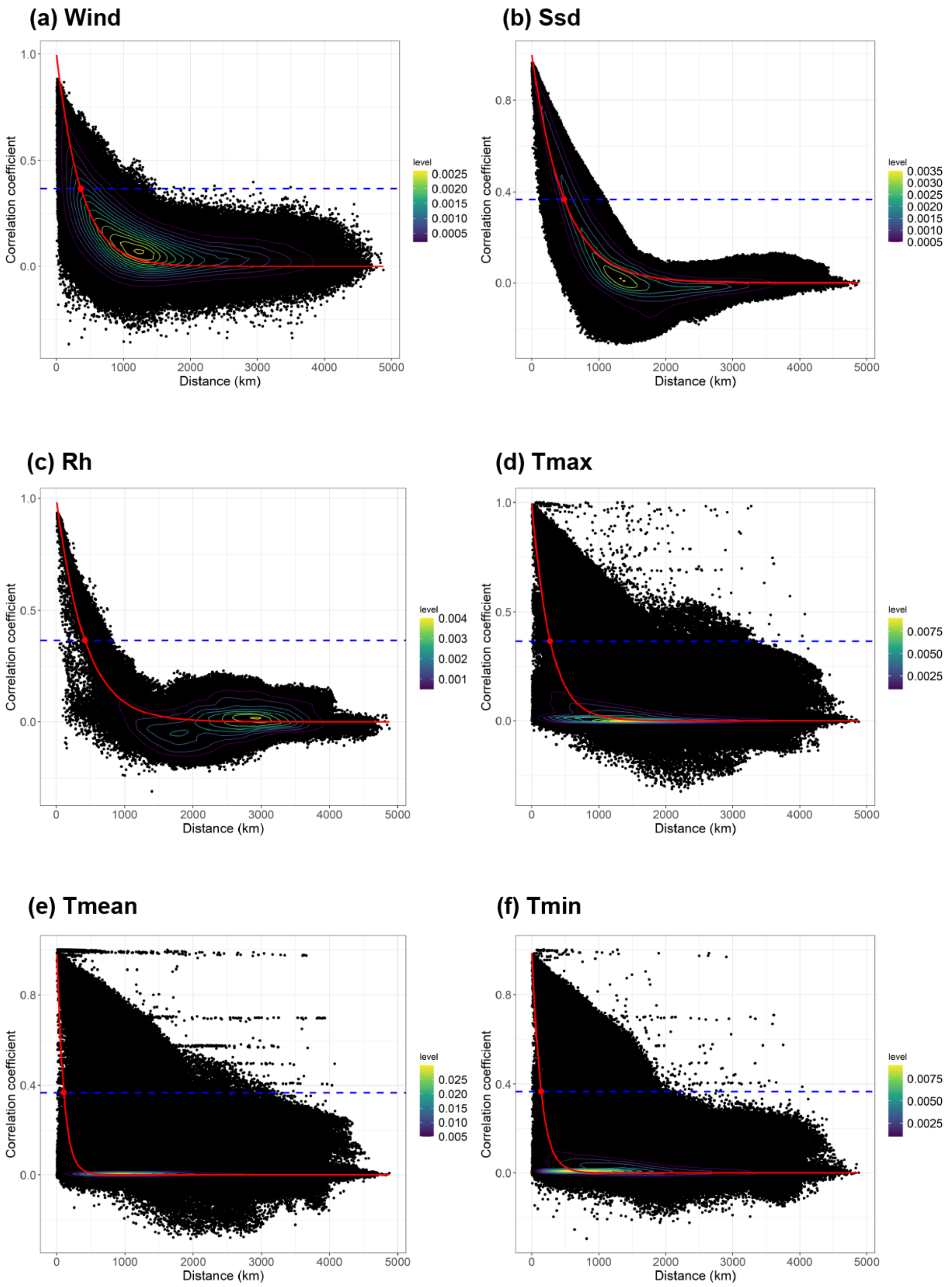

Figure S1: Kernel density visualization of the Correlation Decay Distance (CDD) and the distribution for meteorological variables (Wind≈361, Ssd≈480, Rh≈420, Tmax≈ 272, Tmean≈ 99, Tmin≈ 136) for all stations within the interpolated domain. Black points show the distance–correlation pair for each station. The blue line is the exponential curve fitted to the data by ordinary least squares. The red dashed line marks where correlation equals 1/e.

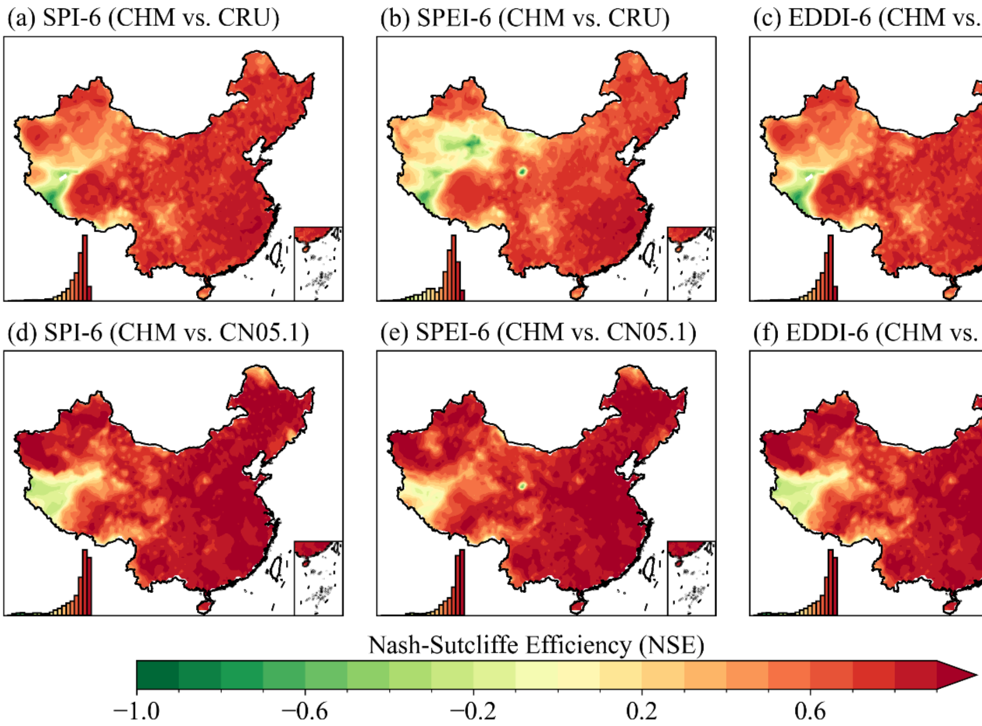

Figure S2: (a–c) Spatial distributions of NSE for SPI-6, SPEI-6, and EDDI-6 based on CHM and CRU data. (d–f) Spatial distributions of NSE for SPI-6, SPEI-6, and EDDI-6 based on CHM and CN05.1 data. The histogram at the bottom left in each subplot shows the distribution of NSE values for all grid cells.

308 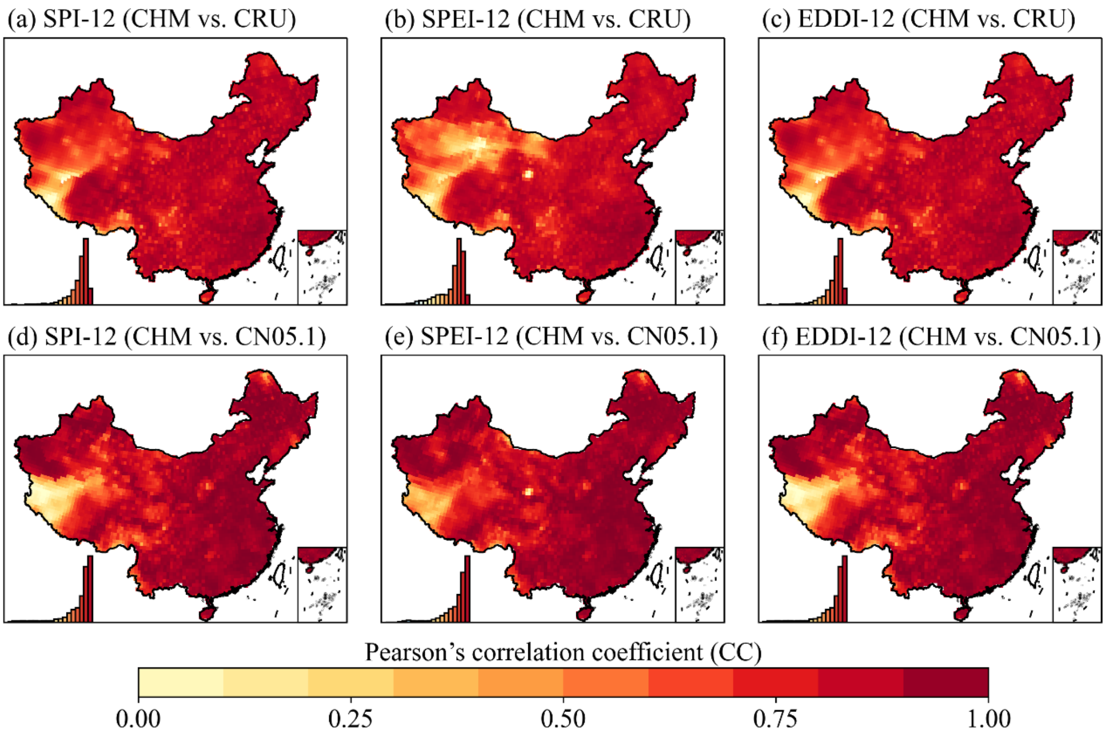

309 **Figure S3**: (a–c) Correlation spatial distributions of SPI-12, SPEI-12, and EDDI-12 based on CHM and CRU data. (d–f) Correlation spatial distributions of SPI-12, SPEI-12, and EDDI-12 based on CHM and CN05.1 data. The histogram at the bottom left in each subplot shows the distribution of correlation coefficients for all grid cells.

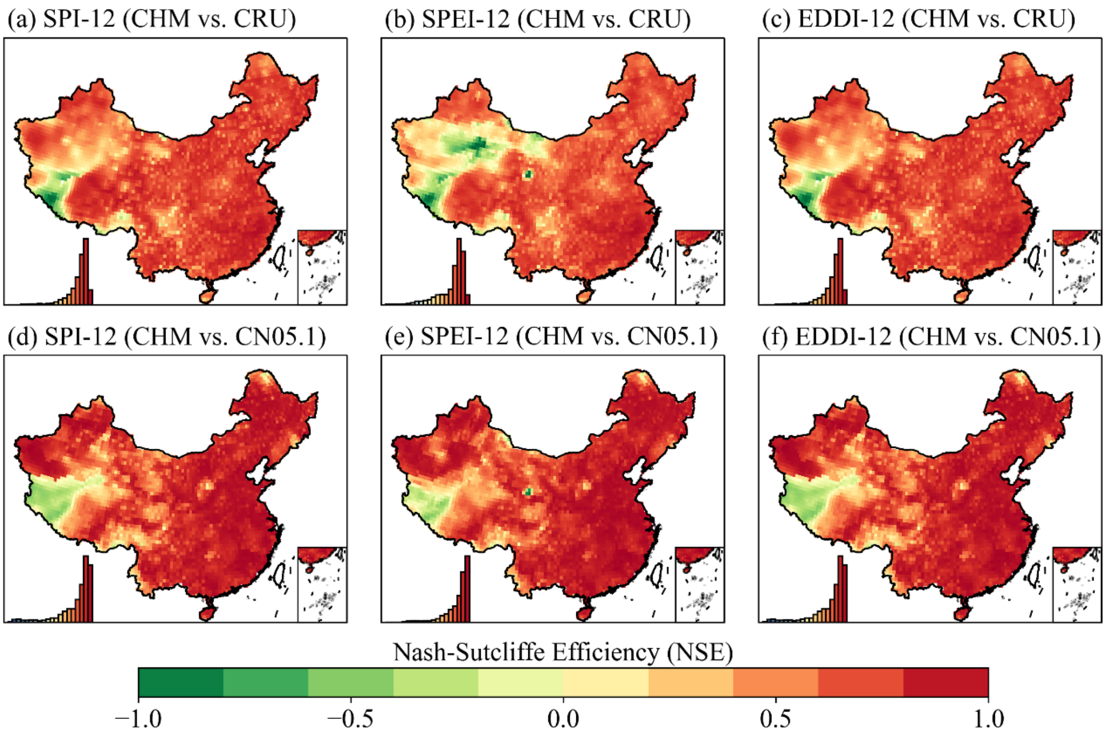

Figure S4: (a–c) Spatial distributions of NSE of SPI-12, SPEI-12, and EDDI-12 based on CHM and CRU data. (d–f) Spatial distributions of NSE of SPI-12, SPEI-12, and EDDI-12 based on CHM and CN05.1 data. The histogram at the bottom left in each subplot shows the distribution of NSE values for all grid cells.

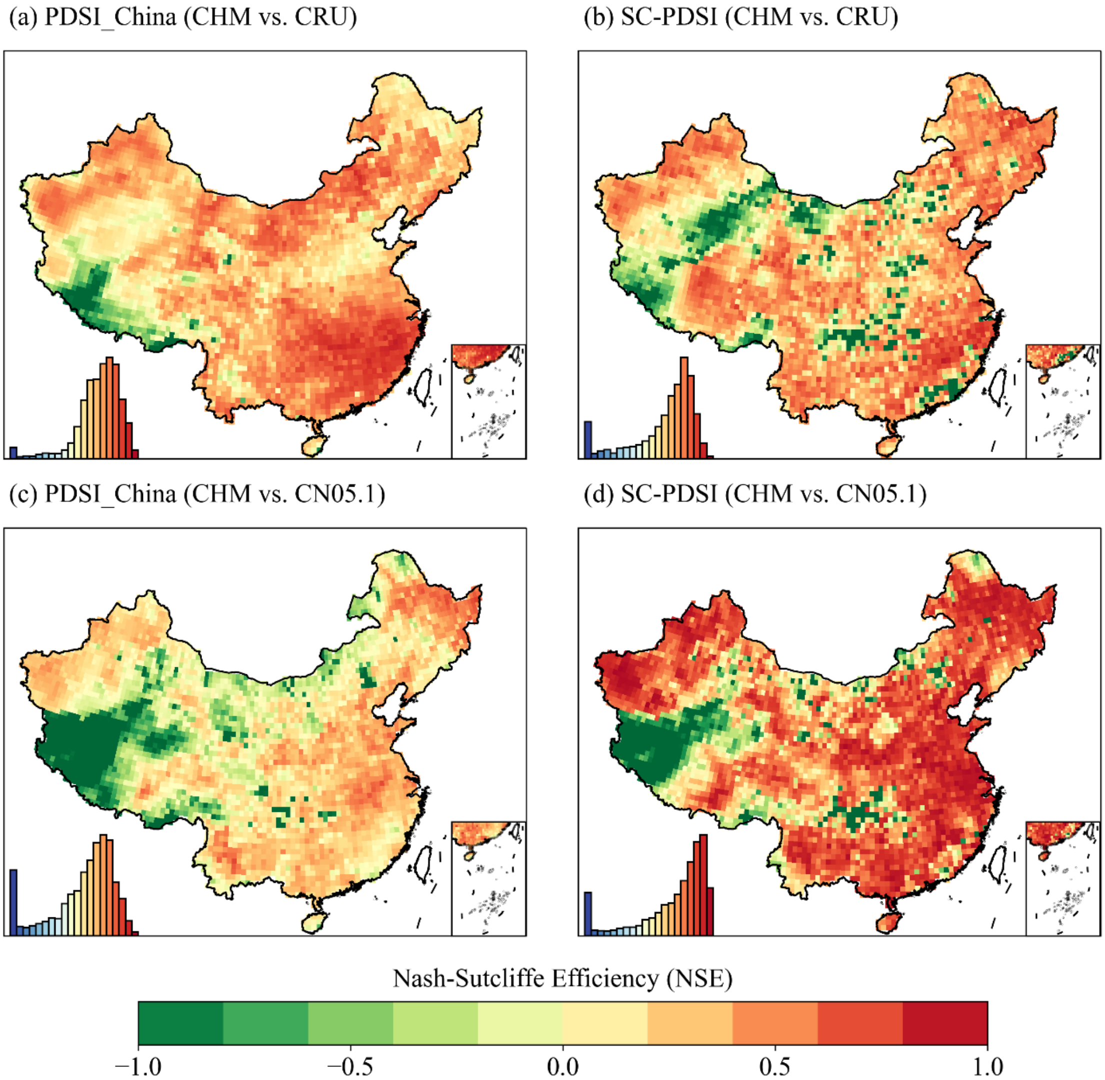

Figure S5: (a, b) Spatial distributions of NSE of PDSI_China and SC-PDSI based on CHM and CRU data. (c, d) Spatial distributions of NSE of PDSI_China, and SC-PDSI based on CHM and CN05.1 data. The histogram at the bottom left in each subplot shows the distribution of NSE values for all grid cells.

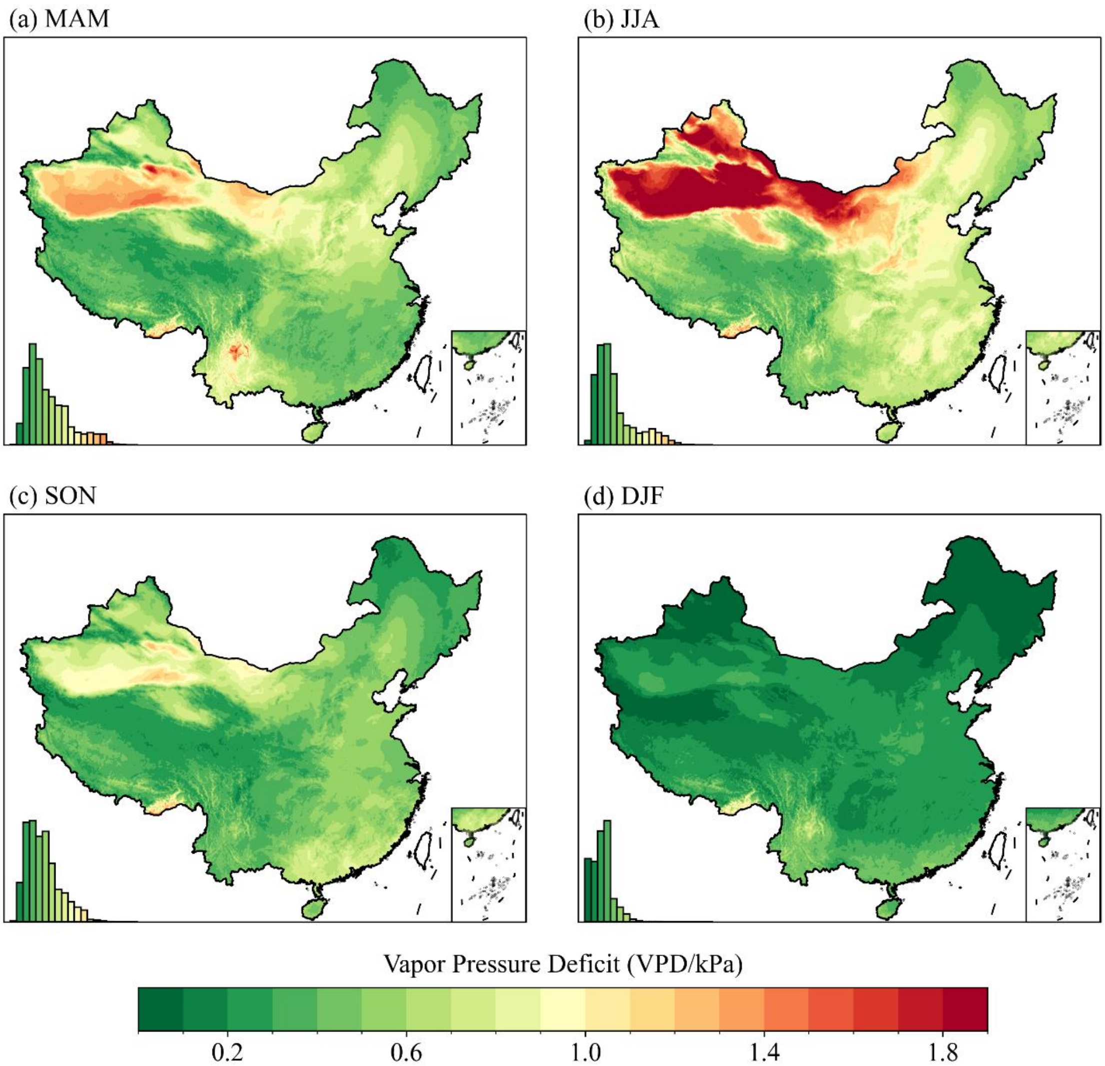

Figure S6: Spatial distribution of seasonal VPD in China, 1961–2022. (a) Spring (March–April–May, MAM). (b) Summer (June–July–August, JJA). (c) Autumn (September–October–November, SON). (d) Winter (December–January–February, DJF). The histogram at the bottom left in each subplot shows the distribution of VPD values for all grid cells.

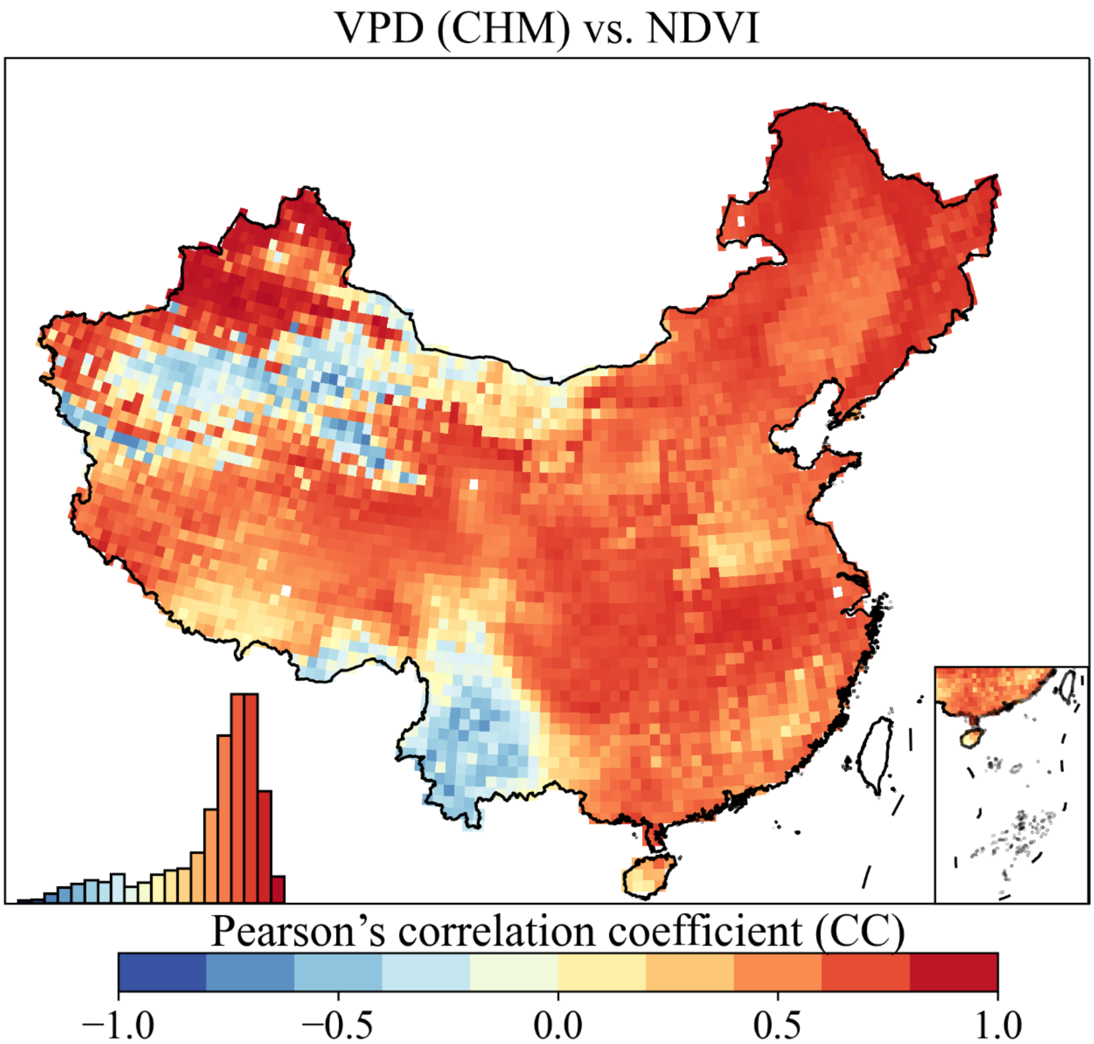

Figure S7: Spatial distributions of correlations between NDVI and VPD based on CHM. The histogram at the bottom left shows the distribution of correlation coefficients for all grid cells.

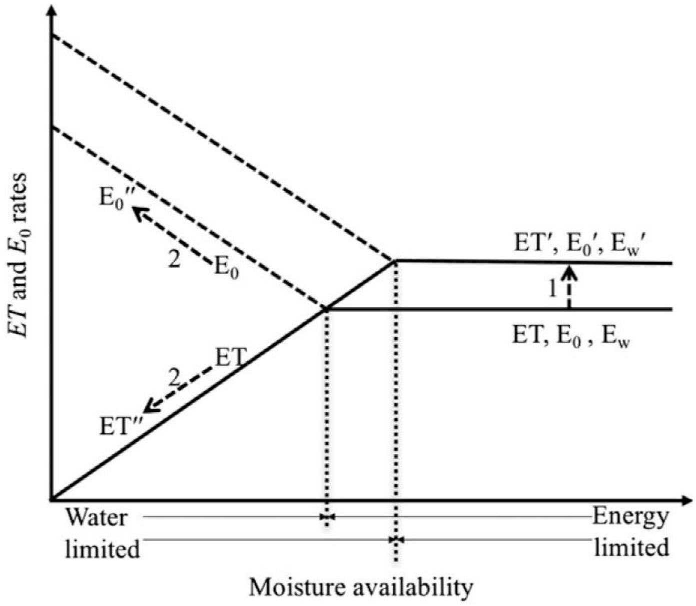

Figure S8: Idealized parallel and complementary responses of AET and ET_0 (E_0 in figure) to varying moisture and energy conditions. Figure adapted from Hobbins et al. (2016).

References

Dai, A., Trenberth, K. E., and Qian, T.: A global dataset of Palmer Drought Severity Index for 1870–2002: Relationship with soil moisture and effects of surface warming, J Hydrometeorol, 5, 1117–1130, https://doi.org/10.1016/j.molcel.2017.04.015, 2004.

Dai, A.: Drought under global warming: a review, Wiley Interdisciplinary Reviews: Climate Change, 2, 45-65, https://doi.org/10.1002/wcc.81, 2011

Dunn, R. J. H., Alexander, L. V., Donat, M. G., Zhang, X., Bador, M., Herold, N., Lippmann, T., Allan, R., Aguilar, E., Barry, A. A., Brunet, M., Caesar, J., Chagnaud, G., Cheng, V., Cinco, T., Durre, I., de Guzman, R., Htay, T. M., Wan Ibadullah, W. M., Bin Ibrahim, M. K. I., Khoshkam, M., Kruger, A., Kubota, H., Leng, T. W., Lim, G., Li-Sha, L., Marengo, J., Mbatha, S., McGree, S., Menne, M., de los Milagros Skansi, M., Ngwenya, S., Nkrumah, F., Oonariya, C., Pabon-Caicedo, J. D., Panthou, G., Pham, C., Rahimzadeh, F., Ramos, A., Salgado, E., Salinger, J., Sané, Y., Sopaheluwakan, A., Srivastava, A., Sun, Y., Timbal, B., Trachow, N., Trewin, B., van der Schrier, G., VazquezAguirre, J., Vasquez, R., Villarroel, C., Vincent, L., Vischel, T., Vose, R., and Bin Hj Yussof, M. N. A.: Development of an updated global land in situ-based data set of temperature and precipitation extremes: HadEX3, J. Geophys. Res.-Atmos., 125, e2019JD032263, https://doi.org/10.1029/2019JD032263, 2020.

Jones, P. D., Osborn, T. J., and Briffa, K. R.: Estimating sampling errors in large-scale temperature averages, J. Climate, 10, 2548–2568, https://doi.org/10.1175/15200442(1997)010<2548:ESEILS>2.0.CO;2, 1997.

Harris, I., Osborn, T. J., Jones, P., and Lister, D.: Version 4 of the CRU TS monthly high-resolution gridded multivariate climate dataset, Sci. Data, 7, 109, https://doi.org/10.1038/s41597-0200453-3, 2020.

Hobbins, M. T., Wood, A., McEvoy, D. J., Huntington, J. L., Morton, C., Anderson, M., and Hain, C.: The evaporative demand drought index. Part I: Linking drought evolution to variations in evaporative demand, J Hydrometeorol, 17, 1745–1761, https://doi.org/10.1175/JHM-D-15-0121.1, 2016.

Hofstra, N. and New, M.: Spatial variability in correlation decay distance and influence on angular-distance weighting interpolation of daily precipitation over Europe, Int. J. Climatol., 29, 18721880, https://doi.org/10.1002/joc.1819, 2009.

Li, L., She, D., Zheng, H., Lin, P., and Yang, Z.-L.: Elucidating Diverse Drought Characteristics from Two Meteorological Drought Indices (SPI and SPEI) in China, J Hydrometeorol, 21, 1513–1530, https://doi.org/10.1175/jhm-d-19-0290.1, 2020.

Mckee, T., Doesken, N., Kleist, J., 1993. The relationship of drought frequency and duration to time scalesProceedings of the 8th Conference on Applied Climatology. American Meteorological Society, Boston, MA.

Mitchell, T. D. and Jones, P. D.: An improved method of constructing a database of monthly climate observations and associated high-resolution grids, Int. J. Climatol., 25, 693–712, https://doi.org/10.1002/joc.1181, 2005.

New, M., Hulme, M., and Jones, P.: Representing twentiethcentury space–time climate variability. part II: development of 1901–96 monthly grids of terrestrial surface climate, J. Climate, 13, 2217–2238, https://doi.org/10.1175/15200442(2000)013<2217:RTCSTC>2.0.CO;2, 2000.

Palmer, W.C., 1965. Meteorological Drought. US Department of Commerce, Weather Bureau, Washington, DC.

Shepard, D. S.: Computer Mapping: The SYMAP Interpolation Algorithm, in: Spatial Statistics and Models, edited by: Gaile, G. L., and Willmott, C. J., Springer

Netherlands, Dordrecht, 133–145, https://doi.org/10.1007/978-94-017-3048-8_7, 1984.

Vicente-Serrano, S. M., Beguería, S., and López-Moreno, J. I.: A multiscalar drought index sensitive to global warming: The standardized precipitation evapotranspiration index, J Clim, 23, 1696–1718, https://doi.org/10.1175/2009JCLI2909.1, 2010.

Wells, N., Goddard, S., and Hayes, M. J.: A self-calibrating Palmer Drought Severity Index, J Clim, 17, 2335–2351, https://doi.org/10.1175/1520-0442(2004)017<2335:ASPDSI>2.0.CO;2, 2004.

Zhong, R., Chen, X., Lai, C., Wang, Z., Lian, Y., Yu, H., and Wu, X.: Drought monitoring utility of satellite-based precipitation products across mainland China, J Hydrol, 568,343–359, https://doi.org/10.1016/j.jhydrol.2018.10.072, 2019.